JOURNAL OF GEOPHYSICAL RESEARCH, VOL. 100, NO. D4, PAGES 7111–7119, APRIL 20, 1995

Gravity waves and turbulence associated with cumulus convection observed with the UHF/VHF clear-air Doppler radars

Kaoru Sato
Center for Climate System Research, University of Tokyo

Hiroyuki Hashiguchi and Shoichiro Fukao
Radio Atmospheric Science Center, Kyoto University, Uji, Japan

Abstract. Vertical wind disturbances are frequently observed during midsummer afternoons in association with cumulus convection. To examine the relation of these wind disturbances to atmospheric stability and turbulence intensity, we carried out intensive observations of wind, temperature and humidity over a large vertical region extending from the boundary layer to the lower stratosphere using UHF/VHF radars and radiosondes at Shiga, Japan (35°N, 136°E). The wind disturbances propagate quickly into the upper troposphere just after 1500 local standard time (LST) when the level of free convection (LFC) descends below the top of the mixed layer, while before that, the disturbances are confined in the mixed layer. However, strong turbulence is largely confined to the region below 3 km even after 1500 LST, suggesting that the height of 3 km corresponds to the top of cumuli, while the wind disturbances above are due to gravity waves generated in association with cumulus convection. In addition, stratospheric disturbances were examined for 12 cases of midsummer disturbances using routine observational data taken with a VHF radar in a height region of 5–24 km. Wind disturbances are observed in the lower stratosphere when turbulence as well as wind disturbances are strong in the whole troposphere. The stratospheric disturbances are dominant in two regions below and above a height of 18 km where the background horizontal wind is weak. Long-period disturbances are observed only in the lower region. This fact suggests that the height of 18 km is a critical level for the long-period gravity waves. The existence of a strong turbulent layer around 18 km is consistent with this inference.

1. Introduction

It is well known that there are eddies such as plumes and thermals which transport heat, momentum, and water vapor in the atmospheric boundary layer. If these eddies penetrate deeply through the condensation level and reach the level of free convection, cumulus clouds form and ascend to greater heights due to the positive buoyancy force arising from condensation heating. Such cumulus convection frequently appears in midlatitude regions during summer afternoons when solar heating has peaked, as also happens in tropical regions over land. However, the small temporal and spatial scales of cumulus convection make its observation very difficult.

Using VHF clear-air radar data from Poker Flat, Alaska (63°N, 147°W), *Nastrom and Gage* [1984] reported a statistically significant diurnal variation in the vertical wind (w) variance which has a maximum in the afternoon during summer. *Sato* [1992], using a VHF radar at Shiga, Japan (35°N, 136°E), called the middle and upper atmosphere (MU) radar, also reported similar vertical wind disturbances which are considered to be due to cumulus convection. Figure 1 shows a contour map of the square of the vertical wind component, hereinafter referred to as w power, in a time-height section during 5 days in midsummer. There was no rainfall during the observation period. Wind disturbances appear every afternoon, propagate upward, and reach the tropopause. Disturbances are observed even in the lower stratosphere on July 9. Using spectral analysis, Sato showed that the vertical wind disturbances are divided into two types, namely, fluctuations with periods shorter than 30 min and longer than 1 hour. The dominance of the longer-period component distinguishes the afternoon disturbances from other kinds of vertical wind disturbances.

The structure of the disturbances in the lower troposphere, however, was not examined, since the data analyzed by *Sato* [1992] covered only the height region of 5–22 km in the upper troposphere and lower stratosphere. Moreover, the shortage of temperature and humidity data prevented further analysis from the viewpoint of atmospheric stability.

Convection is known to be an important source of gravity waves. There are two mechanisms of gravity wave generation [*Clark et al.*, 1986; *Fovell et al.*, 1992; *Alexander et al.*, 1994]: One is the "topographic effect." Convective cells and turrets behave like mountains in the atmosphere when the background wind has significant vertical shear, since the movement of the convective cells and turrets is controlled by

Paper number 95JD00198.
0148-0227/95/95JD-00198$05.00

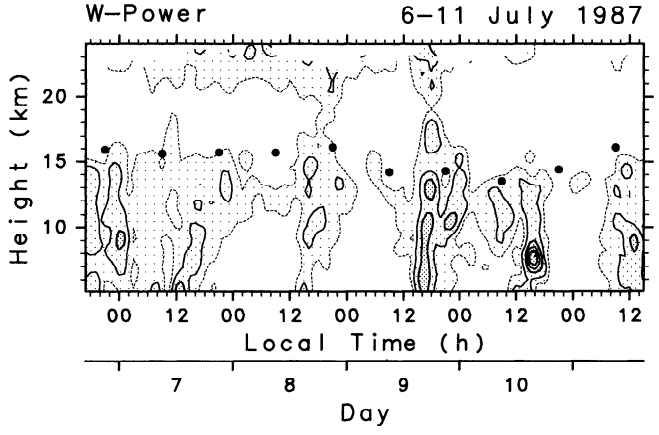

Figure 1. A contour map of w power in a time-height section for July 6–11, 1987, taken from *Sato* [1992]. Smoothing was applied using low-pass filters with a cutoff period of 4 hours in time and a cutoff length of 2 km in vertical. Solid contour intervals are 0.1 m^2 s^{-2}. Dashed curves are the contour of 0.05 m^2 s^{-2}. Circles denote the tropopause.

the low-level wind. Observations of such gravity waves by aircraft and VHF radar have been reported by *Kuettner et al.* [1987] and *Gage et al.* [1989], respectively. The other is the "mechanical oscillator effect." When oscillating updrafts and downdrafts of convective eddies impinge on the tropopause, which is the interface of two layers with different stability, short-period gravity waves are excited. Such short-period gravity waves associated with severe convection are frequently observed during the passage of tropical storms [*Black*, 1977; *Sato*, 1993]. It is possible that some of the afternoon wind disturbances are due to such gravity waves associated with convection.

To examine the structure of the wind disturbances in the lower atmosphere including the boundary layer, we carried out special observations of winds using a boundary layer radar (a UHF clear-air radar, hereinafter referred to as the BL radar) as well as the MU radar. Vertical profiles of temperature and humidity were observed simultaneously using radiosondes at the radar site so as to monitor atmospheric stability. Using routine data taken by the MU radar, we also examine the stratospheric wind disturbances associated with cumulus convection.

2. Wind Disturbances in the Troposphere

2.1. Observations

Winds were observed for about 76 hours on August 25–28, 1992, for a height region of 0.5–24 km by the BL and MU radars. We used three beams of the BL radar for the observation: one beam was pointed vertically and the other two were tilted to the east and north with a zenith angle of 15°. One beam of the MU radar was pointed vertically and four others were tilted to the east, south, west, and north with a zenith angle of 10°. The range resolution in the beam direction and time interval of the observation were 100 m and 1 min for the BL radar and 150 m and about 3 min for the MU radar, respectively. Details of the system of the MU radar and BL radar are described by *Fukao et al.* [1985] and *Hashiguchi et al.* [1994]. Moreover, we observed temperature and humidity every 3 hours by launching radiosondes at the radar site. Nominal height resolution of the radiosonde observations was 10 m.

Since the BL radar is designed for lower-level wind observations, while the MU radar is for upper level observations, we can determine the lowest observable height by the MU radar, which depends on the switching time from transmitter to receiver, by examining the correlation between the time series of winds estimated by both radars at the same level. Figure 2 shows the correlation between 30-min averaged winds observed by the MU radar and those by the BL radar for 0800–2200 LST, August 27 as a function of height. It is seen that the two winds accord well for heights in the range 1.0–1.8 km, indicating that the lowest observable level by the MU radar was 1.0 km. The highest observable level by the BL radar is 1.8 km for this case, although it depends on the atmospheric condition.

Figure 3 shows a time-height section of w power during the whole observation period, using the BL radar data below 1.4 km and the MU radar data above 1.5 km. The data have been smoothed using low-pass filters with a cutoff length of 2 km in height and with a cutoff period of 4 hours in time as in Figure 1. The solid circles indicate tropopause heights estimated from radiosonde observations of temperature. Wind disturbances appear and propagate upward to the upper troposphere in the afternoon of August 26, although wind disturbances on August 27 are confined to the lower atmosphere below 2 km. During the observation period, there was no rain and the weather was calm and very warm. Thus we infer that the disturbances on August 26 are the same kind as those observed in July 1987 shown in Figure 1. From visual observation at the site, cumuli were well developed vertically in the afternoon of August 26, while only undeveloped cumuli were observed on August 27. Therefore it is confirmed that the wind disturbances are associated with cumulus convection as inferred by *Sato* [1992]. In the following sections we investigate the differences between

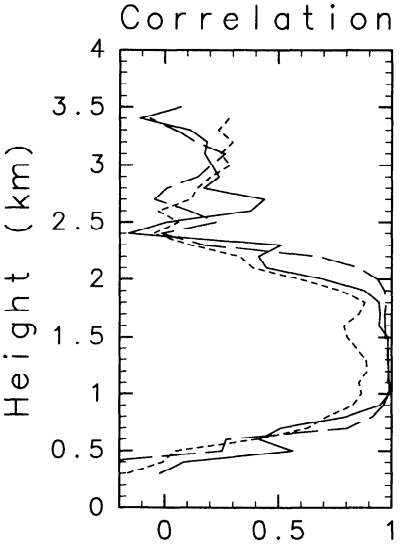

Figure 2. Correlation between 30-min averaged winds from the middle and upper atmosphere (MU) radar and from the boundary layer radar as a function of height. Solid, long-dashed, and short-dashed curves show correlations for zonal, meridional, and vertical wind components, respectively.

August 26 and 27 in terms of the characteristics of the disturbances and atmospheric stability.

Notable are the disturbances at midnight on August 26–27 and 27–28 observed in the BL radar data below 1.4 km in Figure 3. Such disturbances are not observed in the wind profiles below 1.4 km from the MU radar (not shown). The midnight disturbances in Figure 3 are found to be false disturbances, since the winds from the BL radar at midnight on these two occasions are discontinuous with respect to the winds of the MU radar above 1.5 km, while those from the MU radar are continuous. Since we sometimes observe mist in late summer at the MU radar site, it is possible that mist occurred at night during the observation period. The failure in wind estimation by the BL radar may therefore be due to contamination of radar echoes from mist, to which the BL radar is more sensitive than the MU radar.

2.2. Relation With Atmospheric Stability

Development of the mixed boundary layer is examined using radiosonde data. Figure 4 shows vertical profiles of potential temperature θ (thick solid curves), equivalent potential temperature θ_e (thick dashed curves), and the equivalent potential temperature of a hypothetically saturated atmosphere with the same temperature θ_e^* (thin solid curves). Top and bottom panels are for August 26 and 27, respectively. Numerals near the vertical profiles show the local time for the respective observations. Arrows denote the top of the lowest region where θ_e is almost homogeneous, which is likely to correspond to the top of the mixed layer.

The top of the mixed layer can also be inferred from vertical profiles of water vapor mixing ratio. Figure 5 shows the vertical profiles obtained from radiosonde observations. The top of the homogeneous θ_e layer in Figure 4 is also indicated by an arrow for each profile. It is found that the arrows almost exactly indicate the top of a homogeneous layer of the mixing ratio.

The mixed layer deepens gradually until 1500 LST on both days. The difference between the two days occurs after 1800 LST. The homogeneous layer becomes thinner on August 26, while the depth of the homogeneous layer on August 27 remains almost constant.

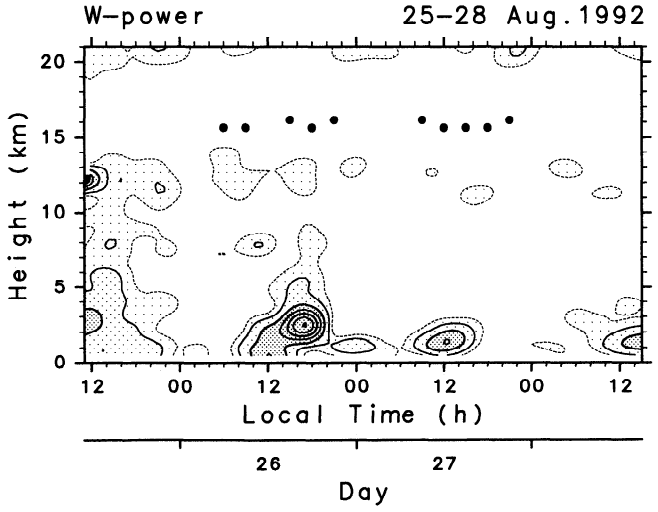

Figure 3. The same as Figure 1 but for August 25–28, 1992.

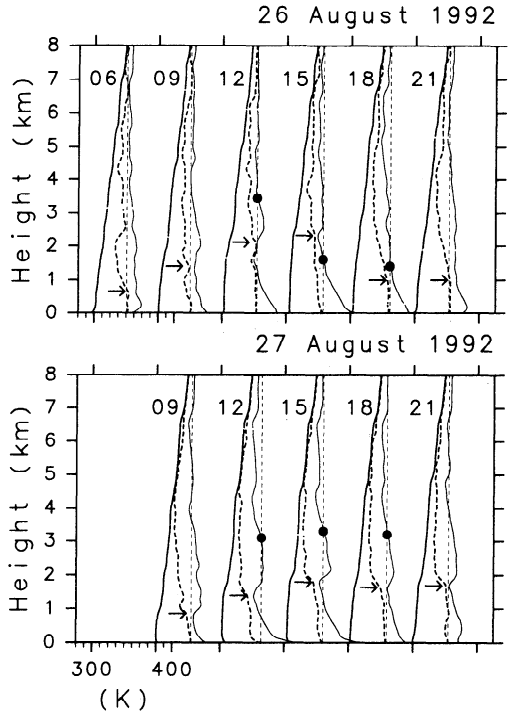

Figure 4. Vertical profiles of θ (thick solid curves), θ_e (thick dashed curves), and θ_e^* (thin solid curves) for August 26 (above) and August 27 (below) 1992. A numeral near each profile shows the local time of the observation. Circles denote the levels of free convection (LFC). Arrows show the top of mixed boundary layer inferred from the vertical profiles of θ_e.

The solid circles in Figure 4 show the level of free convection (LFC), defined as follows: As described briefly in section 1, if an air parcel near the surface z_0 having large $\theta_e(z_0)$ due to solar heating is raised above a level z_{LFC}, i.e., $\theta_e^*(z) \leq \theta_e(z_0)$ for $z \geq z_{\mathrm{LFC}}$, the parcel experiences a buoyant force and tends to propagate farther upward. Thus the level z_{LFC} where $\theta_e^*(z_{\mathrm{LFC}}) = \theta_e(z_0)$ is called the level of free convection. Since we are interested in the stability environment for the wind disturbances propagating toward the upper troposphere, the LFC is defined so that the air parcel near the surface reaches at least a height of 5 km, i.e., $\theta_e^*(z) \leq \theta_e(z_0)$ for $z_{\mathrm{LFC}} \leq z \leq 5$ km. It is important that the LFC descended into the mixed layer at 1500 LST on August 26. This fact suggests that air parcels near the surface were forced by eddies in the mixed layer to rise above the LFC.

The detailed structure of the w power is shown in Figure 6 for August 26 and 27. The cutoffs of the low-pass filters used for smoothing were shortened to 2 hours and 400 m for times and heights, respectively, so as to see detailed time evolution and vertical variation. The top of the mixed layer and the LFC defined above are denoted by triangles and circles, respectively. Until 1500 LST the top of the region with wind disturbances gradually increases and almost accords with that of the mixed layer on both days. Thus it is inferred that the wind disturbances appearing before 1500 LST are due to eddies in the mixed layer. Just after 1500 LST on August 26 when the LFC has dropped below the top of the mixed layer, wind disturbances suddenly develop that penetrate into the upper troposphere. Thus the wind disturbances are probably related to free convective motions

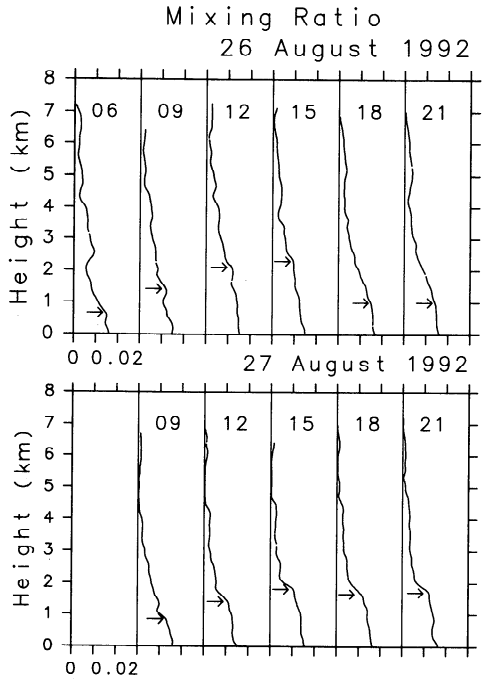

Figure 5. Vertical profiles of water vapor mixing ratio for August 26 (above) and August 27 (below), 1992. A numeral near each profile shows the local time of the observation. Arrows show the top of mixed boundary layer inferred from the vertical profiles of θ_e.

excited in the atmosphere with weak stability. On the other hand, wind disturbances disappear after 1500 LST on August 27 when such an LFC descent is not observed.

It is worth noting that the mixed layer becomes shallower and the mixing ratio gradually decreases with height above the top of the mixed layer after 1800 LST on August 26 (Figure 5). This suggests that the role of wind disturbances changes at around 1500 LST from "mixing" substances in the boundary layer to "transporting" substances toward the upper atmosphere. On August 27, with little wind disturbance after 1500 LST, such a decrease of mixing depth is not observed.

2.3. Turbulence

The turbulent energy dissipation rate (ε), which can be regarded as an index of turbulence intensity, is estimated using the spectral width of the atmospheric echo observed by the BL and MU radars [*Hocking*, 1985]. The spectral width of atmospheric echo may be broadened by effects other than atmospheric turbulence, i.e., the finite beam width of the radar, vertical shear of wind, and short-period gravity waves. These contaminations to the spectral width have been removed by a method introduced by *Hocking* [1985, 1988] so as to obtain accurate values of ε. A specular echo effect [*Hocking*, 1985] was avoided by using only data from oblique beams for the estimation by the MU radar.

Figure 7 shows the time-height section of ε on August 26 and 27. Large values of ε are observed in the mixed layer before 1500 LST on both days. The development of turbulence before 1500 LST on both days and the disappearance of the turbulent region after 1500 LST on August 27 are very similar to the features observed in the wind disturbances (Figure 6). It is reassuring that the ε values are continuous in the vertical around a height of 1.5 km where the estimates by the BL radar and those by the MU radar are connected, bolstering our confidence in the ε estimates. An important difference between turbulence and wind disturbances is that the turbulent region is confined below a height of 3 km after 1500 LST, while wind disturbances reach up to 6 km.

To examine this point more quantitatively, we show a time-height section of the ratio of w power to ε in Figure 8. The contours are drawn with an interval of 3 dB. After 1500 LST on August 26 the ratios below and above 3 km differ by more than 3 dB. This means that the characteristics of wind disturbances change discretely at a height of 3 km in the free atmosphere.

2.4. Spectral Characteristics

Fluctuations of horizontal wind v are next examined in terms of their spectra. *VanZandt* [1982, 1985] showed that if wind disturbances are due to gravity waves and when the background wind is sufficiently weak not to make wave frequencies Doppler-shifted significantly, the frequency power spectrum of $v(P_v(\omega))$ and that of $w(P_w(\omega))$ are related as follows:

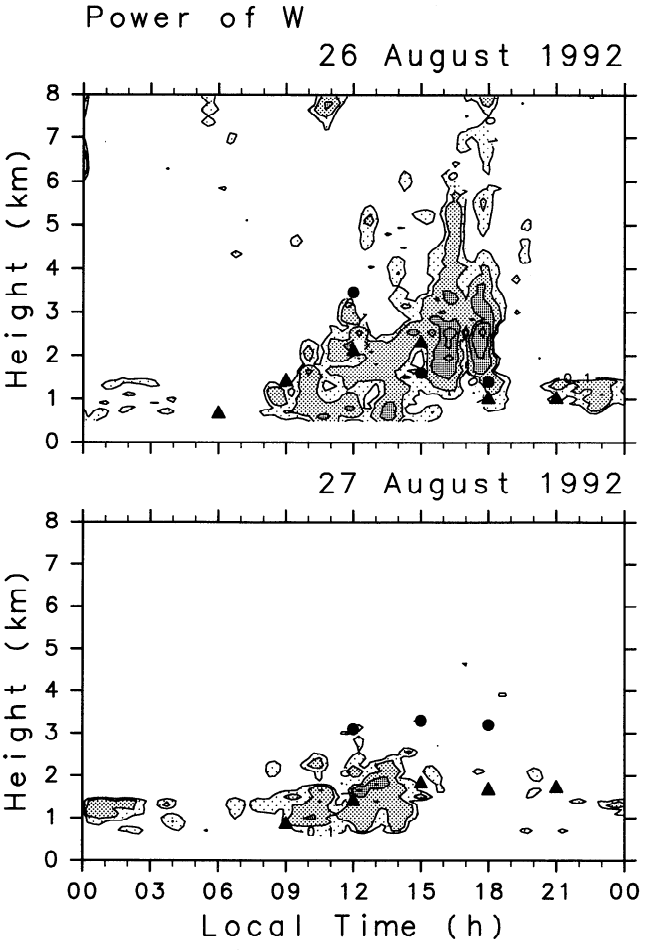

Figure 6. Contour maps of w power in a time-height section for August 26 (above) and August 27 (below), 1992. Smoothing was applied using low-pass filters with a cutoff period of 2 hours in time and a cutoff length of 400 m in vertical. Contours of 0.1, 0.2, 0.5, 1, 2, and 5 $m^2\ s^{-2}$ are drawn. Triangles show the top of mixed layer and circles denote the level of free convection (LFC).

$$\frac{P_v(\omega)}{P_w(\omega)} = \frac{N^2}{\omega^2}, \quad (1)$$

where ω is the wave frequency and N is the Brunt-Väisälä frequency. This relation between $P_v(\omega)$ and $P_w(\omega)$ is derived from the continuity equation and the dispersion relation of gravity waves. Figure 9 shows vertical profiles of the mean horizontal wind and its direction for the daytime (0800–2000 LST) on August 26 (solid curves), the nighttime (2000–0800 LST) on August 26–27 (long-dashed curves), and the daytime (0800–2000 LST) on August 27 (short-dashed curves). Since the background wind is generally weak, the spectrum of wind disturbances is examined using the gravity wave theory.

The spectrum of line-of-sight wind fluctuations observed by an oblique beam $P_{\text{oblique}}(\omega)$ is expressed as

$$P_{\text{oblique}}(\omega) = P_v(\omega) \sin^2 \theta + P_w(\omega) \cos^2 \theta, \quad (2)$$

where θ is the zenith angle. It should be noted that a term related to the covariance of v and w is ignored in (1), since the term is canceled when we average the spectra obtained from a pair of oblique beams having the same zenith angles but azimuth angles differing by 180°, as is done here [see *Sato*, 1990]. The ratio of $P_{\text{oblique}}(\omega)$ to $P_{\text{vertical}}(\omega) \cos^2 \theta (= P_w(\omega) \cos^2 \theta)$, which is the spectrum of vertical winds from a vertical beam weighted by $\cos^2 \theta$, becomes

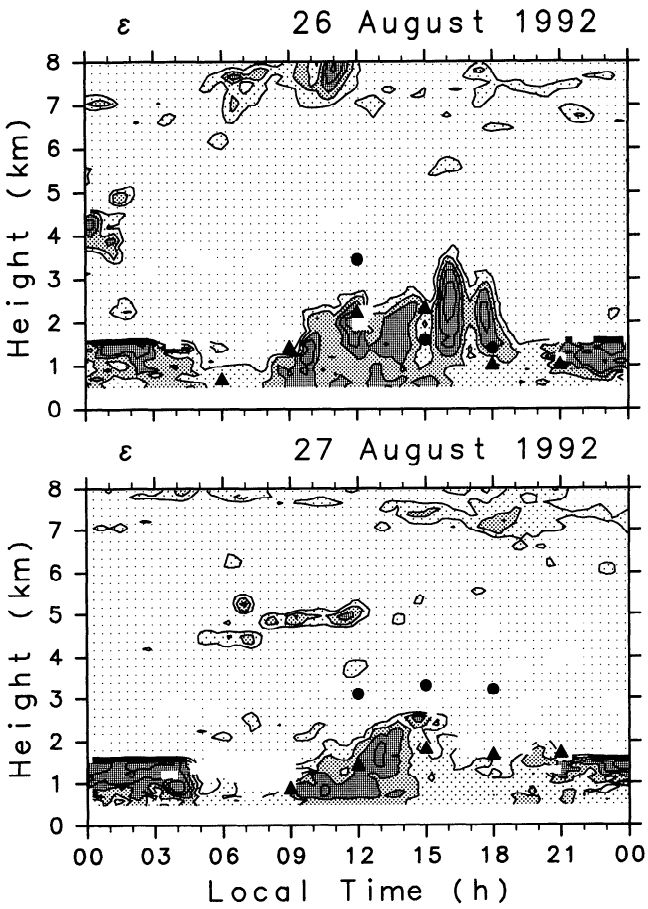

Figure 7. The same as Figure 6 but for the turbulent energy dissipation rate (ε). Contours of 2.5×10^{-4}, 5×10^{-4}, 1×10^{-3}, 2×10^{-3}, and 4×10^{-3} are drawn.

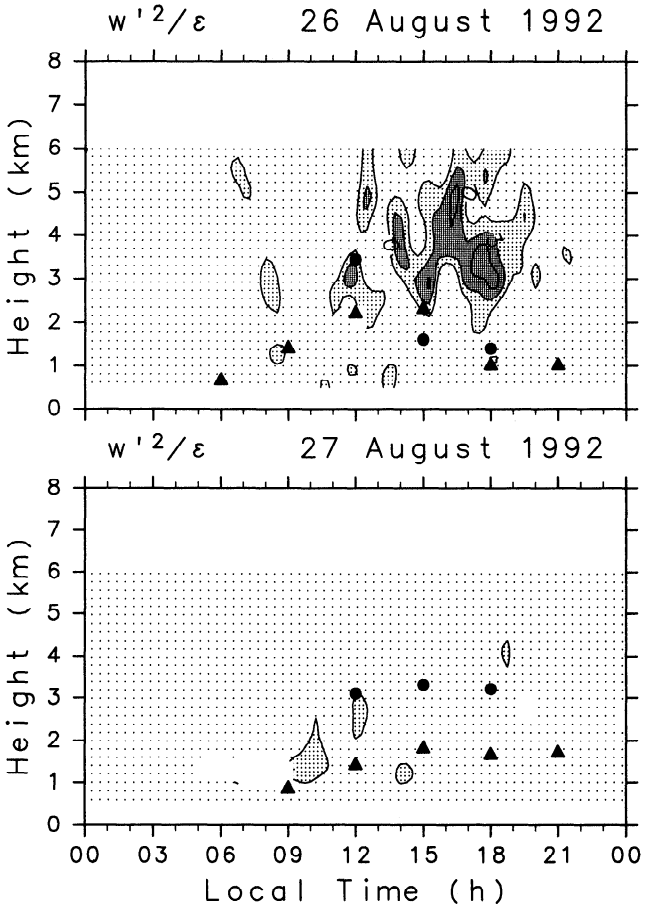

Figure 8. The same as Figure 6 but for the ratio of w power to ε. Contour intervals are 3 dB.

$$\frac{P_{\text{oblique}}(\omega)}{P_{\text{vertical}}(\omega) \cos^2 \theta} = \frac{P_v(\omega)}{P_w(\omega)} \tan^2 \theta + 1 = \frac{N^2}{\omega^2} \tan^2 \theta + 1. \quad (3)$$

Here we assumed homogeneity of the wind variance over the region between the oblique and the vertical beam points. Using a typical Brunt-Väisälä period of 10 min in the troposphere during the observation period, the ratio becomes larger than 2 (3 dB) at periods longer than 1 hour at $\theta = 10°$ used in the MU radar observations.

Using the MU radar data, we obtained the spectra averaged in a height region of 1–3 km corresponding to the mixed boundary layer in the daytime and those averaged for a height region of 3–6 km in the free atmosphere. We did not use the BL radar data because it is not easy to obtain a vertical average of the MU and BL spectra with different frequency intervals. Figure 10 shows the spectra in the daytime on August 26, the nighttime on August 26–27, and the daytime on August 27. Dashed and solid curves show $P_{\text{oblique}}(\omega)$ and $P_{\text{vertical}}(\omega) \cos^2 \theta$, respectively. Arrows indicate the period of 1 hour, at which the difference of the two spectra should become about 3 dB if the spectra are due to gravity wave motions following VanZandt's theory. The nighttime spectra in both lower and upper regions accord well with VanZandt's theory, i.e., departure between $P_{\text{oblique}}(\omega)$ and $P_{\text{vertical}}(\omega) \cos^2 \theta$ is distinct at periods longer than 1 hour, indicating that the wind fluctuations in the

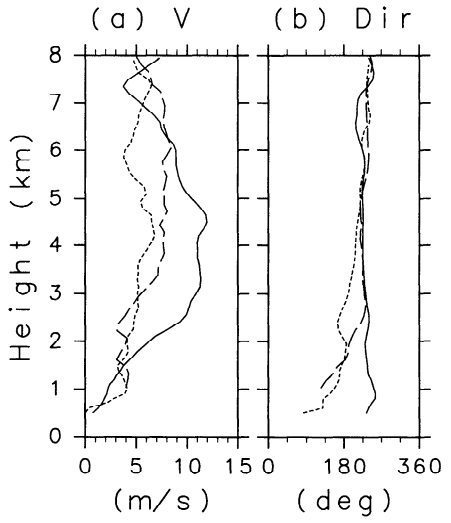

Figure 9. (a) Speed and (b) direction of the mean horizontal wind as a function of height for 0800–2000 LST 26 (solid curves), 2000 LST 26–0800 LST 27 (long-dashed curves), and 0800–2000 LST 27 (short-dashed curves), August 1992.

nighttime are likely due to gravity waves. This is the case for the spectra for the upper region in the daytime on August 27 in which wind disturbances were not observed. On the other hand, we do not observe such a departure for the daytime spectra for the mixed layer (the lower region) on both August 26 and 27. One possibility is the effect of moisture condensation associated with cumulus development, which may make N^2 approach zero locally. In such an environment with inhomogeneous stability we cannot apply the universal gravity wave spectral theory discussed by VanZandt. The spectra are instead considered to be due to well-developed eddy motions in the mixed layer.

Interesting are the spectra in the height region 3–6 km in the daytime of August 26 when strong wind disturbances reached the upper troposphere. The spectra are very similar to those in the mixed boundary layer and not explained by VanZandt's gravity wave theory. However, we cannot attribute the wind disturbances to eddies in cumulus convection, since turbulence was very weak in this region.

2.5. Possible Interpretation of Disturbances Above 3 km on August 26

During the daytime of August 26 the turbulent region was confined below a height of 3 km, while the wind disturbances were strong up to the upper troposphere. The discrete transition in the turbulence intensity means the dominance of different kinds of disturbances below and above 3 km. One likely interpretation is that the height of 3 km corresponds to the top of cumuli, and the disturbances observed above are due to gravity waves generated in association with the cumulus convection.

At first glance, this interpretation seems to contradict the spectral characteristics which could not be explained by VanZandt's gravity wave theory. However, as is discussed by *Sato* [1990], when gravity waves are generated by a particularly strong generation mechanism, such as occurs, for example, with mountain waves, the wave energy contaminates the spectra at frequencies far from the wave frequencies. In such a case, the spectral characteristics are significantly different from those expected from the simple theory of VanZandt's. As mentioned in section 1, it is known that convective eddies and turrets behave like topography in the background wind having vertical shear and generate gravity waves [e.g., *Clark et al.*, 1986; *Kuettner et al.*, 1987]. According to Figure 9 the mean horizontal wind in the afternoon of August 26 has a relatively large vertical shear of 4×10^{-3} s^{-1} in a height region of 1–3 km, indicating that gravity waves are probably generated due to the topographic effect of cumulus convection. The dominance of long-period components found in the power spectra in Figure 10 is consistent with this interpretation of quasi-stationary gravity waves.

3. Wind Disturbances in the Stratosphere

3.1. Data Description

Sato [1992] showed that vertical wind disturbances during midsummer afternoons are sometimes observed even above the tropopause. The disturbances in the stratosphere are considered to be due to gravity waves generated in association with cumulus convection. In this section we examine the stratospheric disturbances in terms of their relation to tropospheric disturbances and their spectral characteristics. MU radar data are used for summer days in which afternoon disturbances were observed. There were 12 cases, August 19–20, 1986, July 6–9, 1987, August 4–6, 1987, September 8 and 10, 1987, and August 26, 1992. The beam directions of the observations are the same as those of the MU radar observations mentioned in section 2. The data cover the height region 5–24 km at an interval of 150 m. The time interval of the observations is about 2–3 min. The tropopause, which is estimated using temperature data from routine radiosonde observations in Shionomisaki (150 km south of the MU radar site), is located in a height region of 14–16 km for most of the 12 cases.

3.2. Relation to Wind Disturbances in the Troposphere

Figure 11 shows a composite of the time-height sections of w power for the 12 cases. Wind disturbances appear at

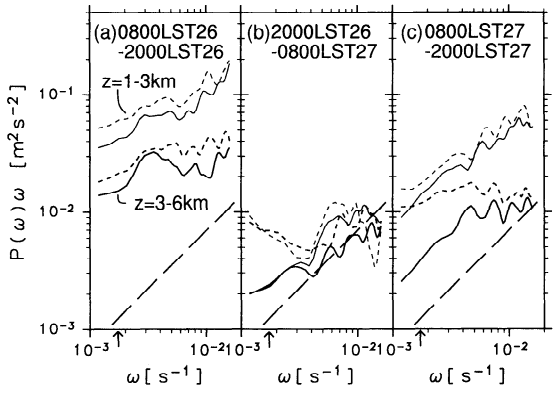

Figure 10. Frequency power spectra in an energy content form of w fluctuations from a vertical beam weighted by $\cos^2 \theta$ (solid curves), where θ is the zenith angle of oblique beams (=10°) and spectra of line-of-sight wind fluctuations of oblique beams (dashed curves) for periods of (a) 0800–2000 LST 26, (b) 2000 LST 26–0800 LST 27, and (c) 0800–2000 LST 27, August 1992. Thick and thin curves are for height regions of 3–6 km and 1–3 km, respectively.

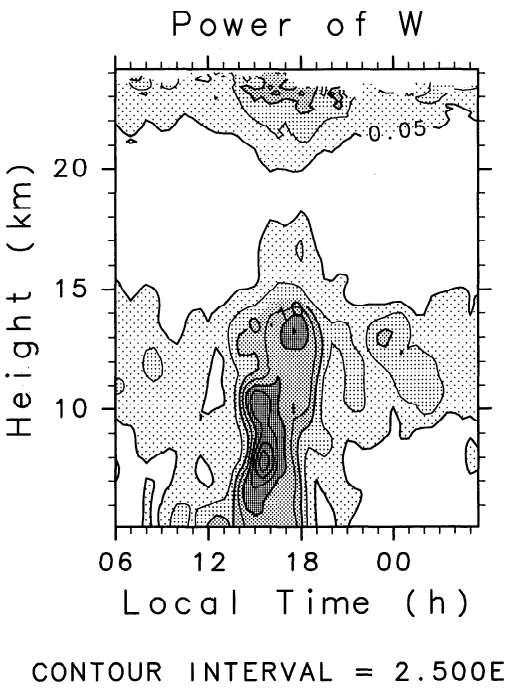

Figure 11. A composite of time-height sections of w power for 12 cases when the midsummer disturbances are observed in the troposphere. Contour intervals are 0.025 m^2 s^{-2}.

around 1400 LST and reach the tropopause around 1700 LST. Disturbances in the stratosphere are enhanced at around 1700 LST and dominant in two height regions, i.e., below 17 km and above 19 km. Judged from the timing of the enhancement, it is considered that the disturbances in the stratosphere are related to the tropospheric disturbances.

Figure 12 is a scatter diagram for variances of vertical winds in the troposphere and in the stratosphere. The variances are calculated for a period from 1300 to 1900 LST at each height and averaged for a height region of 5.4–15 km for the troposphere and of 16–22 km for the stratosphere. Positive correlation is observed between the two variances, suggesting again the connection between the disturbances in

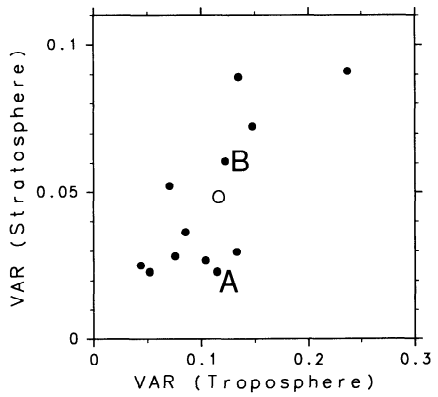

Figure 12. A scatter diagram for variances of w fluctuations in the troposphere (5.4–15 km) and the stratosphere (16–22 km). Units of horizontal and vertical axes are m^2 s^{-2}. The open circle shows the average of the 12 cases. "A" and "B" denote the cases of August 19, 1986, and July 7, 1987, respectively.

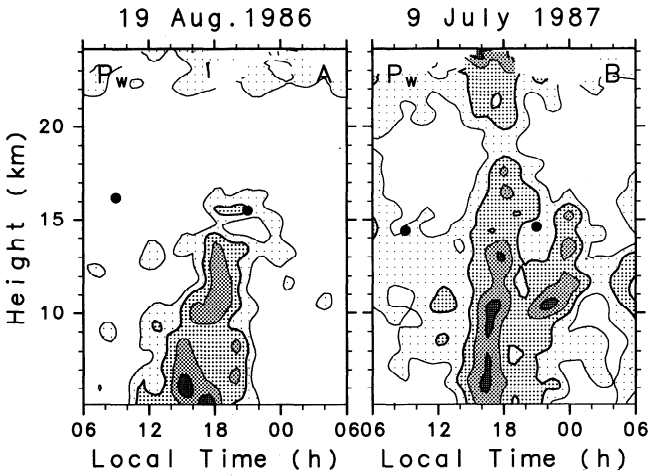

Figure 13. A contour map of w power for cases A (August 19, 1986) and B (July 7, 1987). Contours of 0.03, 0.06, 0.13, and 0.25 m^2 s^{-2} are drawn. Circles denote the tropopause estimated from vertical profiles of temperature at Shionomisaki (about 150 km south of the MU radar site) by routine radiosonde observations.

the troposphere and in the stratosphere. However, the correlation is not very large. For example, for cases with variances in the troposphere of 0.1–0.15 m^2 s^{-2} the ratio of the maximum to minimum variances in the stratosphere is about 4. We therefore examined in detail the difference in the characteristics of the wind disturbances between the two cases August 19, 1986 (A), and July 7, 1987 (B), which have almost the same variances in the troposphere but variances in the stratosphere that differ by about a factor of 3.

Time-height sections of w power for cases A and B are presented in Figure 13. Stratospheric disturbances are observed only in case B, although there is little difference between the two cases in the intensity and upward propagation (from a height of 5 km at 1500–1600 LST to the tropopause level of about 15 km at 1700–1800 LST) of tropospheric disturbance.

It is noted that a disturbance is also observed in the period from 2000 LST on July 9, 1987, to 0000 LST on July 10, 1987, in the upper troposphere in case B. Generation of the disturbance is probably related to the large vertical shear observed in the background wind (not shown). A detailed examination of this disturbance is beyond the scope of our study, however.

Figure 14 shows the turbulent energy dissipation rate ε in a time-height section for the cases A and B. The contour intervals are the same as in Figure 7. Regions where the estimation could not be made because of insufficient data quality are unhatched. For case B, large ε values are observed in a time-height region where the wind disturbances were dominant in the troposphere, while ε values are very small for case A.

This suggests that the tropospheric disturbances are due to gravity waves for case A and due to cumulus convection for case B. It is, therefore, inferred that tropospheric gravity waves for case A were generated in association with convection below the lowest observed height of 5 km, as in the case of August 26, 1992, in section 2.3, and that the strong gravity waves in the stratosphere for case B were generated

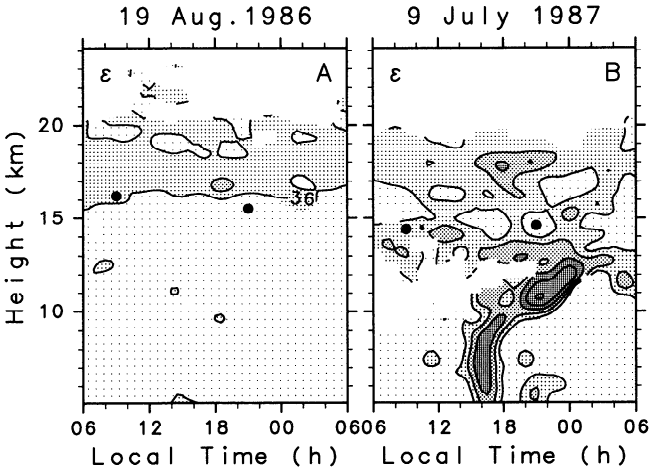

Figure 14. The same as Figure 12 but for ε. Contour intervals are taken to be the same as in Figure 7.

by cumulus convection which was sufficiently strong to reach the tropopause.

Similar enhancement of turbulence in the troposphere is observed in other cases having strong disturbances in the stratosphere (not shown).

3.3. Spectral Characteristics

It is known that the w spectra of $P_w(\omega)$ usually have a shape proportional to ω^0 in a calm atmospheric condition [*Ecklund et al.*, 1986]. This spectral shape implies the dominance of fluctuations having higher frequencies when we discuss the spectra in its energy content form $P_w(\omega)\omega$. *Sato* [1992] showed that tropospheric disturbances in the afternoon have large energy at frequencies lower than $2\pi/(30$ min) as well as at higher frequencies, although the spectra in the morning when disturbances are not observed have a shape of ω^0 similar to Ecklund et al.'s cases. Figure 15 shows frequency spectra as a function of height for the period 1500–2000 LST on July 9, 1987 (case B), when midsummer disturbances are observed both in the troposphere and in the stratosphere. Below the tropopause level of 15 km, power tends to be large for periods longer than 2×10^3 s, as shown by *Sato* [1992]. Long-period components are dominant also in a height region up to 18 km in the stratosphere. Above 19 km, however, spectral densities at long periods are small and short-period fluctuations are relatively dominant. As shown in Figure 13, the w power is maximized in two height regions, below 17 km and above 19 km in the stratosphere. It is seen from Figure 15 that the minimum in the w power observed around 18–19 km is mainly attributed to decrease of the variance of long-period fluctuations. Similar differences in spectral characteristics between the upper and lower height regions are also observed for other cases with stratospheric disturbances (not shown).

Next, let us consider the reason why the long-period disturbances disappear above 18–19 km. As discussed in the previous section, the long-period disturbances are likely due to gravity waves generated by the topographic effect of cumulus convection. The disappearance at a height of 18–19 km may be due to approach to the critical level. Although there are no wind data in the lower troposphere for case B, the background wind is generally weak in summer, so that phase speeds of the gravity waves should be very small.

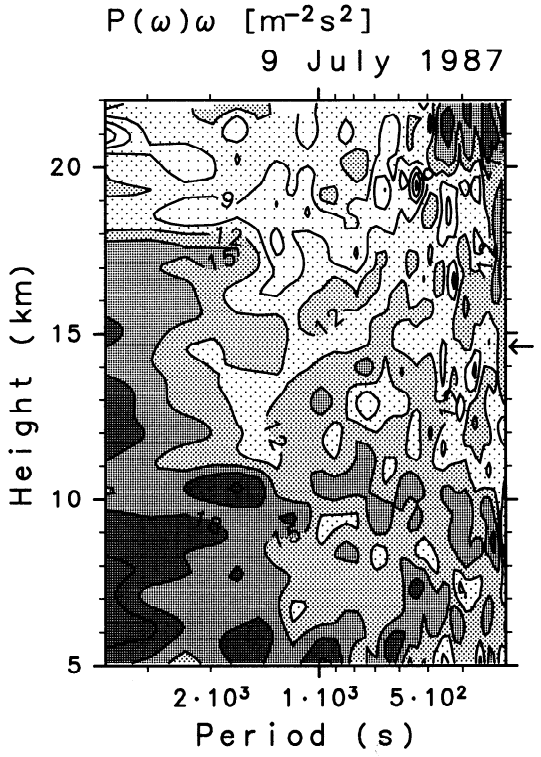

Figure 15. Power spectra of w fluctuations for case B as a function of height. Labels on contours denote values of 10 times logarithm of the spectral density with a base of 10. The arrow shows the location of the tropopause.

Figure 16 shows the vertical profiles of ε, the magnitude of horizontal wind V, and w power averaged for 1400–1800 LST for case B. It is found that the background horizontal wind is weak around 18–19 km where the w power is minimized. This is consistent with the feature around the critical level for quasi-stationary waves like mountain waves. Moreover, it is worth noting that the turbulent energy dissipation rate has a peak around 18 km. This supports the speculation that the breaking of gravity waves occurs near the critical level.

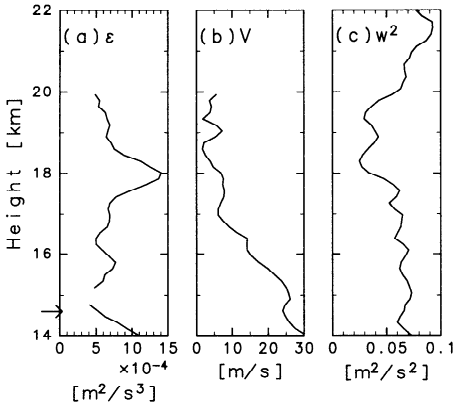

Figure 16. Vertical profiles of (a) ε, (b) the magnitude of background horizontal wind, and (c) w power for case B. The arrow shows the location of the tropopause.

4. Summary and Concluding Remarks

It is known that vertical wind disturbances appear in the afternoon in midsummer and propagate upward, up to, and sometimes beyond the tropopause. We made special observations using the MU radar, BL radar, and radiosondes to examine the relation of the midsummer disturbances to the background atmospheric stability and turbulence intensity for 76 hours in the summer of 1992. Strong wind disturbances were observed on August 26 when cumuli were well developed. The disturbances reached the upper troposphere within a few tens of minutes after 1500 LST when the LFC descended below the top of the mixed boundary layer (~2 km). This fact indicates that the midsummer disturbances are related to cumulus convection which is generated by solar heating. Even after 1500 LST, the turbulence intensity was strong only below 3 km and not in the whole region where the wind disturbances were dominant. It is inferred that the height of 3 km corresponded to the top of cumuli, and the wind disturbances above were due to gravity waves generated over cumuli.

Moreover, we examined wind disturbances in the lower stratosphere using data for 12 days when afternoon disturbances were observed in the troposphere. It was found that the wind disturbances appear in the lower stratosphere when both the wind disturbances and the turbulence are strong in the whole troposphere. The intensity of stratospheric disturbances was commonly minimum around a height of 18–19 km where the background horizontal wind was very weak. This is mainly due to disappearance of long-period fluctuations above 18–19 km. A strong turbulent layer at around 18–19 km suggests that breaking of the long-period gravity waves occurred there.

The gravity waves having short periods from a few minutes to a few hours associated with cumulus convection are considered to be important for transport of momentum and substances across the tropopause because the waves are associated with strong vertical motions. Using geostationary meteorological satellite data, *Nitta and Sekine* [1994] reported recently the presence of convective activity having diurnal or semidiurnal cycles in the tropical regions. Quantitative evaluation of the role of short-period gravity waves is necessary to understand the transport processes, in particular in the tropical region where convective activity is strong.

Acknowledgments. The MU radar belongs to and is operated by the Radio Atmospheric Science Center of Kyoto University. The present authors thank Rechard Fovell, Kenneth S. Gage, and two anonymous reviewers for their valuable comments. Thanks are extended to Thomas L. Bell for kindly checking our English in the manuscript.

References

Alexander, M. J., J. R. Holton, and D. R. Durran, The gravity wave response above deep convection in a squall line simulation, *J. Atmos. Sci.*, in press, 1994.

Black, P. G., Some aspects of tropical storm structure revealed by hand-held camera photographs from space, in *Skylab Explores the Earth, NASA SP-380*, pp. 417–461, 1977.

Clark, T. L., T. Hauf, and J. P. Kuettner, Convectively forced internal gravity waves: Results from two-dimensional numerical experiments, *Q. J. R. Meteorol. Soc.*, *105*, 945–962, 1986.

Ecklund, W. L., K. S. Gage, G. D. Nastrom, and B. B. Balsley, A preliminary climatology of the spectrum of vertical velocity observed by clear-air Doppler radar, *J. Clim. Appl. Meteorol.*, *25*, 885–892, 1986.

Fovell, R., D. Durran, and J. R. Holton, Numerical simulations of convectively generated stratospheric gravity waves, *J. Atmos. Sci.*, *49*, 1427–1442, 1992.

Fukao, S., T. Sato, T. Tsuda, S. Kato, K. Wakasugi, and T. Makihira, The MU radar with an active phased array system, 1, Antenna and power amplifiers, *Radio Sci.*, *20*, 1155–1168, 1985.

Gage, K. S., W. L. Ecklund, and D. A. Carter, Convection waves observed using a VHF wind-profiling Doppler radar during the pre-storm experiment, Preprint Volume, in *24th Conference on Radar Meteorology*, pp. 705–708, American Meteorological Society, Boston, Mass., 1989.

Hashiguchi, H., S. Fukao, T. Tsuda, M. D. Yamanaka, D. L. Tobing, T. Sribimawati, S. W. B. Harijono, and H. Wiryosumarto, Observations of the planetary boundary layer over equatorial Indonesia with an *L*-band clear-air Doppler radar: Initial results, *Radio Sci.*, in press, 1995.

Hocking, W. K., Measurement of turbulent energy dissipation rates in the middle atmosphere by radar techniques: A review, *Radio Sci.*, *20*, 1403–1422, 1985.

Hocking, W. K., Two years of continuous measurements of turbulence parameters in the upper mesosphere and lower thermosphere made with a 2-MHz radar, *J. Geophys. Res.*, *93*, 2475–2491, 1988.

Kuettner, J. P., P. A. Hildebrand, and T. L. Clark, Convection waves: Observations of gravity wave systems over convectively active boundary layers, *Q. J. R. Meteorol. Soc.*, *113*, 445–467, 1987.

Nastrom, G. D., K. S. Gage, A brief climatology of vertical wind variability in the troposphere and stratosphere as seen by the Poker Flat, Alaska, MST radar, *J. Clim. Appl. Meteorol.*, *23*, 453–460, 1984.

Nitta, T., and R. Sekine, Diurnal variation of convective activity over the tropical western Pacific, *J. Meteorol. Soc. Jpn.*, *72*, 627–641, 1994.

Sato, K., Vertical wind disturbances in the troposphere and lower stratosphere observed by the MU radar, *J. Atmos. Sci.*, *47*, 2803–2817, 1990.

Sato, K., Vertical wind disturbances in the afternoon of midsummer revealed by the MU radar, *Geophys. Res. Lett.*, *19*, 1943–1946, 1992.

Sato, K., Small-scale wind disturbances observed by the MU radar during the passage of Typhoon Kelly, *J. Atmos. Sci.*, *50*, 518–537, 1993.

VanZandt, T. E., A universal spectrum of buoyancy waves in the atmosphere, *Geophys. Res. Lett.*, *9*, 575–578, 1982.

VanZandt, T. E., A model for gravity wave spectra observed by Doppler sounding systems, *Radio Sci.*, *20*, 1323–1330, 1985.

S. Fukao and H. Hashiguchi, Radio Atmospheric Science Center, Kyoto University, Uji 611, Japan.

K. Sato, Center for Climate System Research, 4-6-1, Komaba, Meguro-ku, Tokyo 153, Japan.

(Received August 3, 1994; revised January 13, 1995; accepted January 13, 1995.)